VISSR ATMOSPHERIC SOUNDER

Monthly Progress Report No. 4
For the period 1 Dec. 1973 to 31 Dec. 1973

Contract No. NAS5-21965

For National Aeronautics and Space Administration
Goddard Space Flight Center
Glen Dale Road
Greenbelt, Maryland 20771

by

V. E. Suomi, Principal Investigator
L. A. Sromovsky, Co-Investigator

The University of Wisconsin
Space Science and Engineering Center
1225 West Dayton Street
Madison, Wisconsin 53706

TABLE OF CONTENTS

I. Introduction

During the past month work has slowed significantly as a result of Christmas Holidays, vacations and temporary manpower shifting to other projects. The picture should improve somewhat in January, and considerably in February, as additional manpower is brought into the project.

Items reported on for December are (1) studies of operation modes and (2) simulation of a procedure for correction of N-S misalignment of InSb and HgCdTe detector arrays. Other work in process includes in-flight calibration analysis and data processing procedure simulation.

II. Operation Modes

In December the VAS processor specifications and latitude stepping requirements were changed to provide capabilities to image during retrace and to dwell sound with non-overlapping complete spatial coverage (this is discussed in the November progress report (#3) on NAS5-21965; see Figure 7 of that document). Given the choice between slow retrace (1 step/spin) with imaging and fast retrace (10.677 steps/spin) without imaging, a question arises concerning the most efficient way to operate the VAS. For sounding as well as imaging scanning efficiency requires serious consideration.

The main limitation of rapid retrace (10X), and rapid forward scan as well, is that it introduces significant spin axis nutation which degrades the precision image geometry required for wind determinations and precise registration of sounding channels. Thus, following any rapid (10X) latitude stepping a waiting period of approximately 6.5 min is required to insure that the nutation is sufficiently damped. This waiting period is not required for the normal stepping rate because the nutation it introduces is negligible. A comparison of these two retrace rates is made in Figure 1 on the basis of total time between downward scanned frames. Times are computed according

Figure 1 Center to center time spacing between downward scanned frames for slow (1X) and fast (10X) retrace rates

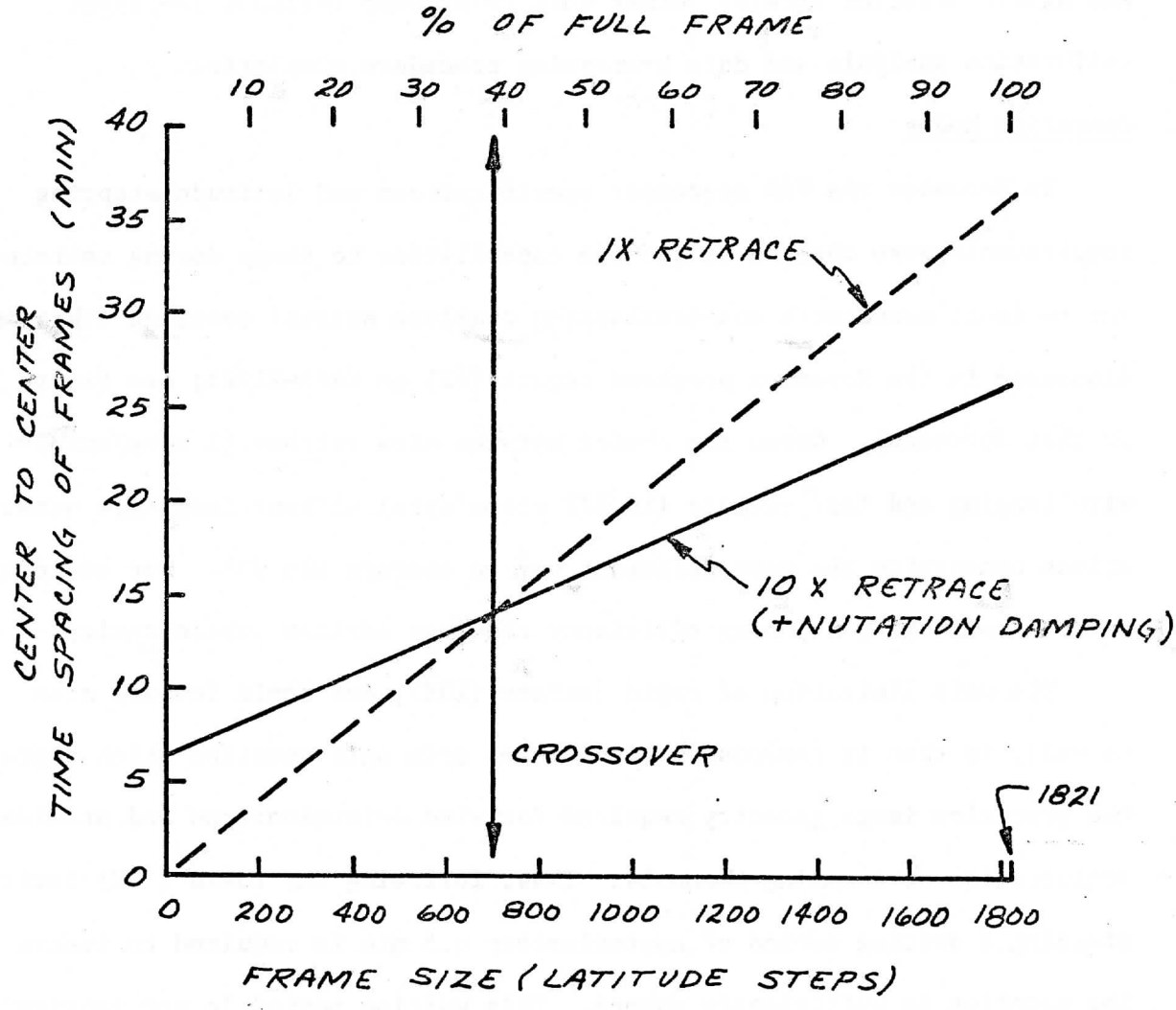

to the formulae

$$\Delta t_{10X} = (\text{frame size}) \times \left(\frac{19.9 \text{ min}}{1821 \text{ lines}} \right) + 6.5 \text{ min}$$

$$\Delta t_{1X} = (\text{frame size}) \times \left(\frac{36.4 \text{ min}}{1821 \text{ lines}} \right)$$

where the frame size is in terms of IR lines (0.192 mr latitude steps). As indicated in Figure 1, the slow retrace is more efficient than fast retrace for small frames (< 700 IR lines) and less efficient for large frames (> 700 IR lines). However, this comparison is somewhat weighted against the slow retrace since the fact that it produces an upward scanned image for every downward scanned image has been neglected. If we consider both images equally useful (both separately and as pairs) then the slow retrace is more efficient than fast retrace for all frame heights. Even at 100% of full frame it produces images at a rate of two/36.4 min while fast retrace yields images at a rate of two/52.8 min.

The variety of patterns for repetitive scanning of the full disc is enormous if upward and downward scanned images are possible. The standard full frame scan mode is shown in Figure 2(a), an alternative possibility is shown in Figure 2(b). In many respects the second option has distinct advantages over the first among which are the following: (1) no "dead" time is required to wait for nutation damping; and (2) 4 half frame images are obtained in a short period of time (36.4 min) allowing more reliable tracking of short lived cloud tracers and rapidly changing mesoscale features. Other points of comparison are made in Table 1.

At this time neither of these two modes is meant to be recommended. Instead, the alternate modes are merely suggested for consideration. The optimum scanning method will depend on precise operational requirements and data processing procedures to be employed. To see how these constraints can affect available time for dwell sounding, let us consider the following

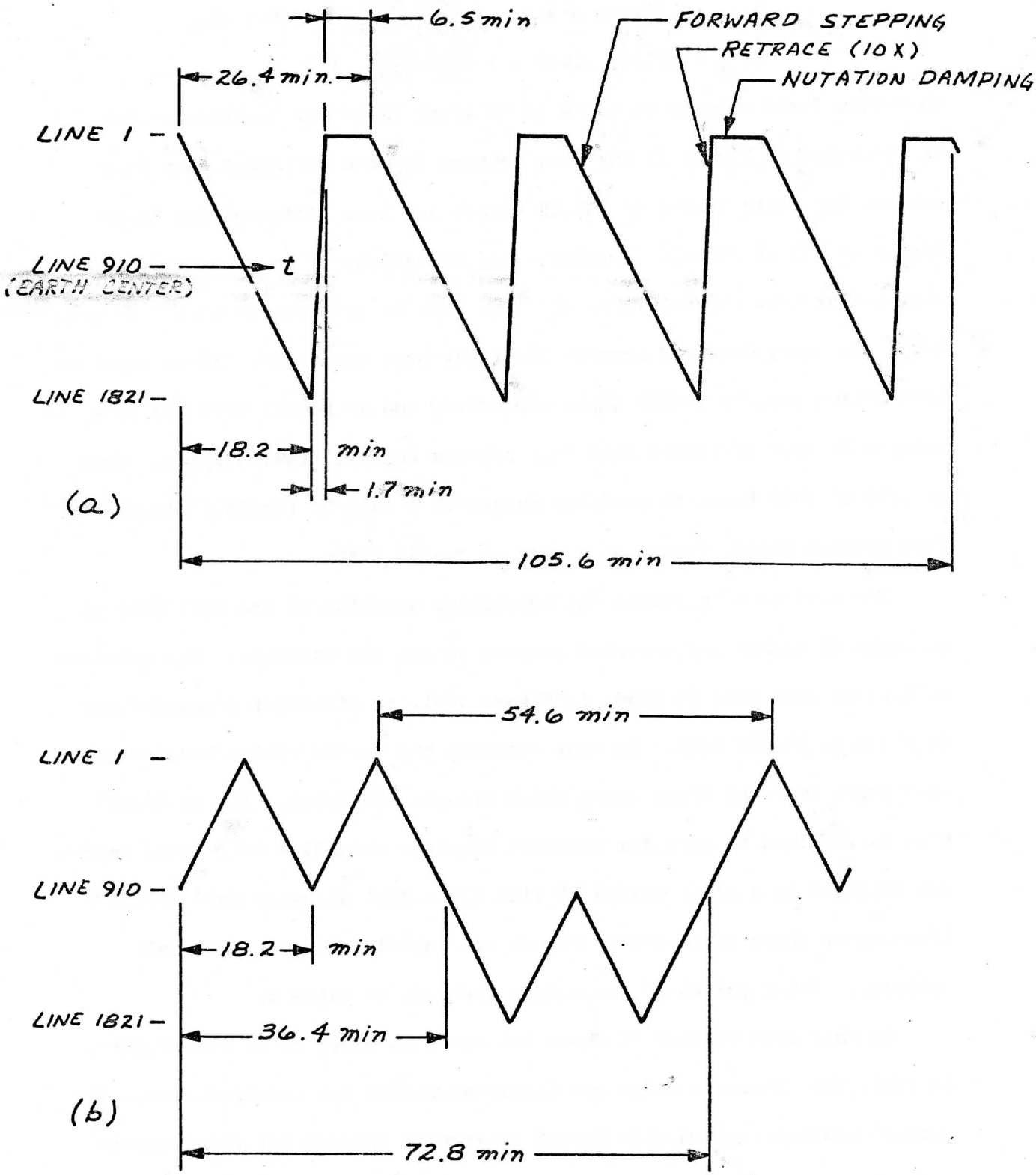

Figure 2 Alternate repetitive scan patterns for imaging (a) standard format, (b) MV variant.

Table 1 Comparison of Two Image Scanning Modes

	(a) full frame 10X retrace	(b) M-W alternating 1/2 frame with 1X retrace imaging
time between downward scanned full frame images	26.4 min	72.8 min
center to center time between full frame images	26.4 min	36.4 min
Total time to obtain a four frame sequence for a hemisphere	105.6 min	36.4 min
Center to center time between images scanned in same direction	26.4 min	18.2 min
Center to center time between adjacent images	26.4 min	9.1 min

set of imaging requirements as valid (for the sake of argument):

(1) full frame down scanned images required @ ≃ 1 hour (but fixed) intervals for movie loops of large scale motions, and

(2) 4 image sequences for synoptic wind sets required @ ≃ 6 hour intervals.

The ways in which these requirements can be met for (a) and (b) modes of scanning are charted in Figure 3. The characteristics of these modes are also summarized in Table 2. It should be noted that for all time periods for which dwell sounding takes place the scan pattern would deviate from that shown in Figure 3. The only implied constraint on scanning for dwell sounding is that the line no. at the end of this period must be 1(one), i.e. some of the dwell sounding time period is required to position the VISSR scan mirror for the next downward scanned image frame.

Because some sounding time must be spent in mere translation from bottom to top of frame positions the effective sounding time can become very short if the total time is broken into very small segments. In order to describe this numerically it is first necessary to determine the most efficient procedure for N-S translating to the area to be sounded and then, after sounding, to N-S translate to the top of frame position.

Figure 4 compares the translation efficiency of three different methods for achieving the following motion program:

(1) translate from 1821 to L + ΔL

(2) stay at L + ΔL until nutation is damped

(3) sound from L + ΔL to L

(4) translate from L to 1

(5) stay at 1 until nutation is damped

The three translation times depicted in Figure 4 are for (1), (2), (4) and (5) only and for the following approaches for retrace rates:

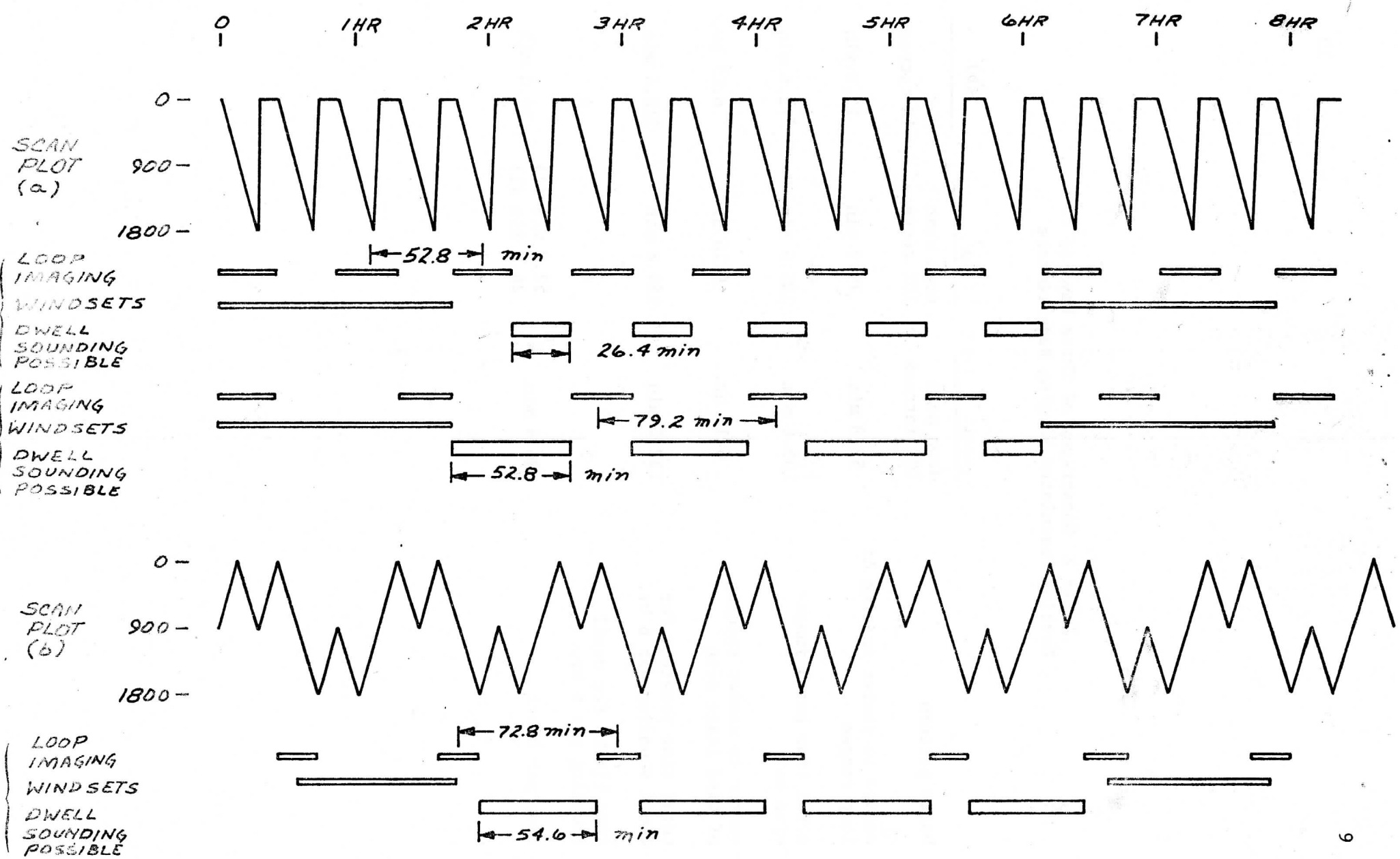

Figure 3 Comparison of three approaches to meeting postulated operational imaging constraints. Horizontal bars denote time used or available for corresponding functions.

Table 2 Comparison of Three Ways of Meeting Postulated Imaging Requirements

	(a_1)	(a_2)	(b)
basic pattern	down scan 10X retrace	down scan 10X retrace	M-W 1X retrace
center to center spacing of loop images	52.8 min	79.2 min	72.8 min
total time per 4 image wind set	105.6 min	105.6 min	72.8 min
center to center spacing of wind image sets	6.16 hr.	6.16 hr.	6.07 hr.
total time possible for dwell sounding per 6 hr.	132.0 min	184.8 min	218.4 min
time blocks for dwell sounding per 6 hr.	5	4	4
time per block	26.4 min	52.8 min (3) 26.4 min (1)	54.6 min

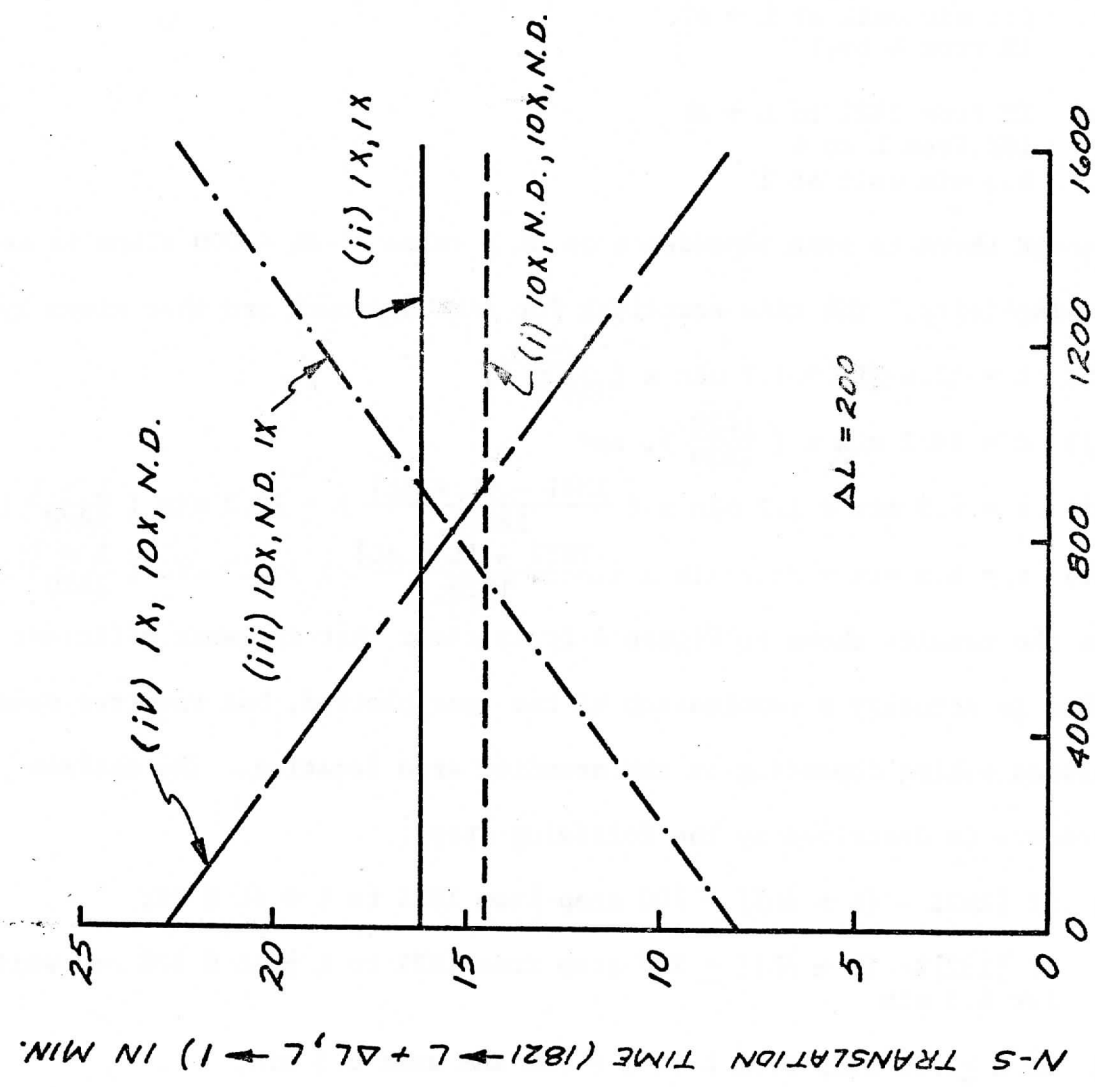

Figure 4 Comparison of translation times as a function of L for 1821 → L + ΔL, L → 1, with sounding over the latitude band ΔL. Sounding times are not included.

(i) 10X from 1821 to L + ΔL
6.5 min wait at L + ΔL
10X from L to 1
6.5 min wait at 1

(ii) 1X from 1821 to L + ΔL
1X from L to 1

(iii) 10X from 1821 to L + ΔL
6.5 min wait at L + ΔL
1X from L to 1

(iv) 1X from 1821 to L + ΔL
10X from L to 1
6.5 min wait at 1

Although there is some dependence on ΔL a value of ΔL = 200 lines is assumed for simplicity. The time equations for each approach are then given by:

(i) $t = 13.0 \text{ min} + 1.7 \text{ min} \times \left(\frac{1620}{1820} \right)$,

(ii) $t = 18.2 \text{ min} \times \left(\frac{1620}{1820} \right)$, and

(iii) $t = 6.5 \text{ min} + 1.7 \text{ min} \times \left(\frac{1821 - [L + \Delta L]}{1820} \right) + 18.2 \text{ min} \left(\frac{L - 1}{1820} \right)$, and

(iv) $t = 6.5 \text{ min} + 18.2 \text{ min} \times \left(\frac{1821 - [L + \Delta L]}{1820} \right) + 1.7 \text{ min} \left(\frac{L - 1}{1820} \right)$.

From the results shown in Figure 4 it is clear that the most efficient method is actually a combination of the four plotted, but requires some decision making depending on the sounding area location. The optimum procedure is described by the following steps:

(1) if $[1821 - (L + \Delta L)] > 700$ step from 1821 to L + ΔL @ 1X;

if $[1821 - (L + \Delta L)] \leq 700$ step from 1821 to L + ΔL @ 10X and wait for 6.5 min

(2) if $L \geq 700$ step from L to 1 @ 10X and wait 6.5 min;

if $L < 700$ step from L to 1 @ 1X

In order to determine how much time is available for sounding as a function of the total time within continued block we must solve the equation

$$t_{BLOCK} = t_{TRANS} + t_{SOUND}$$

The sounding time t_{SOUND} depends on required spins/dwell and the scan pattern used. For this discussion we will use the parameters listed in Table 3.

Table 3 Dwell Sounding Scan Parameters

spins/dwell	76
sounding coverage/dwell	0.768 mr (equivalent to 4 latitude steps)
avg. spins/dwell for stepping	4
avg. total spins/dwell	80
avg. total spins/step	20
avg. stepping period	0.2 min/step

The scanning program chosen for dwell sounding consists of the following steps:

(1) dwell sound upward from L + ΔL to L @ 10 spins/step average (this provides half the required spin budget);

(2) image downward from L to L + ΔL @ 1 spin/step; and

(3) dwell sound upward from L + ΔL to L @ 10 spins/step average (this provides the second half of the total required spin budget).

This program was chosen instead of a single pass in order to provide an image pair from which cloud motions and vertical structure can be determined. This mode takes only 10% more time than a single pass. The time equation for the double pass is: $t_{SOUND} = (0.21 \text{ min/line})\Delta L$. For simplicity let us assume $1 < L < 700$. Then the equation to be solved for ΔL is just

$$t_{BLOCK} = 6.5 \text{ min} + 1.7 \text{ min} \times \left(\frac{1821 - [L + \Delta L]}{1820} \right) + .01 \text{ min} \times (L - 1) + .21 \text{ min} \times \Delta L$$

provided that $L + \Delta L < 1121$ (always true for cases considered here while $L < 700$). The equation can be simplified to the form

$t_{BLOCK} = 8.2 \text{ min} + L \times (.01093 \text{ min}) + \Delta L(0.21093 \text{ min})$, or

$$\Delta L = \frac{t_{BLOCK} - 8.2 \text{ min} - .01093 \text{ min} \times L}{0.21093 \text{ min}} .$$

Results for ΔL as a function of t_{BLOCK} are presented in Figure 5 for a selection of L values. Referring to Figure 5 and Table 3 it is possible to determine the sounding efficiency of the three scan modes shown in Table 4. The dramatic differences apparent there underline the significance of careful optimization of scan programs to meet operational requirements.

III. Registration Errors: A Correction Algorithm Evaluated

The relative North-South alignment of the InSb detector array with the HgCdTe array (discussed in the November Progress Report on NAS5-21965) is likely to be no better than $\pm$ 15μr including improvements obtained from cooler rotation. This amounts to 7.8% of the small detector FOV, and 3.9% of the large detector FOV.

A possible means to partially correct for this shift between the two arrays, specifically between the large InSb detectors and the small HgCdTe elements, is to form linear combinations of small detector FOV's to achieve a shift in the N-S position of the HgCdTe spatial weighting functions which is equivalent to the shift due to misalignment. With perfect registration it would be possible to average four 0.192 mr FOV's (two on each line) to obtain the same spatial weighting as one 0.384 mr InSb detector FOV. With imperfect N-S registration the procedure would be to use six 0.192 mr FOV's in a weighted average, four being the same FOV's used previously, and the two additional FOV's would come from the adjoining line in the same direction as the relatively shifted InSb array. These latter FOV's would be weighted by the factor $\delta/0.192$ mr and the former by $1 - \delta/0.192$ mr (δ being the angular shift between arrays).

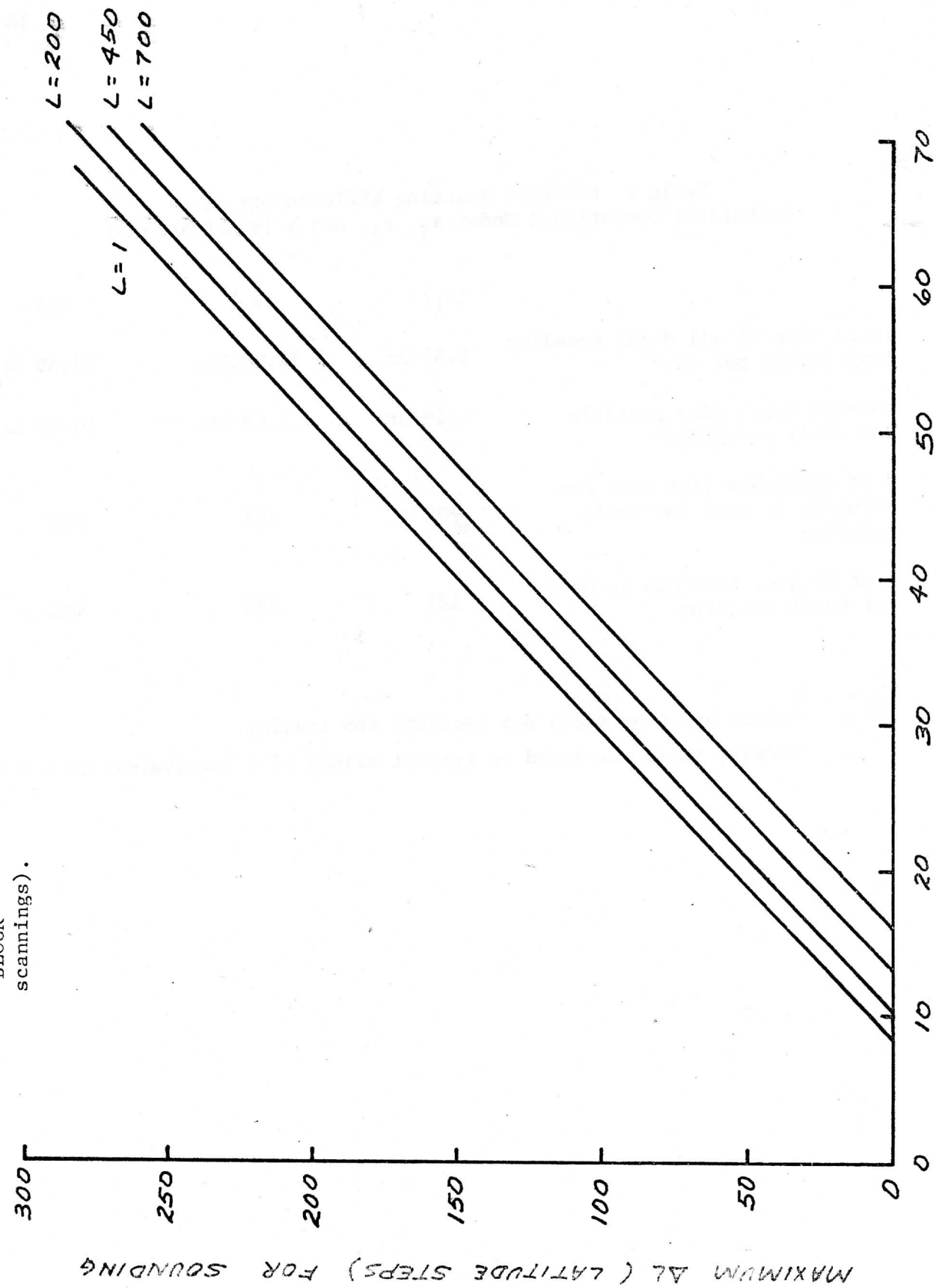

Figure 5 Latitude swath (ΔL) that can be dwell sounded under postulated operational constraints as a function of t_{BLOCK} (the continuous time available between image scannings).

Table 4 Relative Sounding Efficiencies of Postulated Operational Modes a_1, a_2, and b (see Figure 3)

	(a_1)	(a_2)	(b)
total time of all dwell sounding time blocks per day*	8.57 hr.	12.00 hr.	14.39 hr.
average total time possible for dwell sounding**	4.29 hr.	7.69 hr.	10.88 hr.
% of available time that can actually be used for dwell sounding	50%	64%	76%
% of 24 hrs. that can be used for dwell sounding	18%	32%	45%

NOTES: *These are time slots not required for imaging.

**These times are based on typical values of L (equivalent to L = 450).

In order to see the sizes of errors produced by the misregistration and the degree of improvement possible with the correction algorithm, a computer simulation was made with realistic data derived from Gemini photographs and adjacent soundings. Details of the simulation procedure and its results can be found in the appendix. The major conclusions are summarized in Table 5.

Table 5 Test of Algorithm for Correcting N-S Misregistration (Canary Islands Data)

RMS Radiance error resulting from 15μr error in registration	0.50 erg/(s-cm^2-ster-cm^{-1})
RMS Radiance error after correction	0.20 erg/(s-cm^2-ster-cm^{-1})

These results do not include radiometric errors due to noise or other factors. While the improvement shown by the correction algorithm is significant the final error is still too large to be acceptable. Some restriction of the averaging area to larger sizes may be required if better alignment cannot be achieved.

APPENDIX A

Simulation of an Algorithm to Reduce North South Detector Registration Errors

by

Ralph DeDecker

January 1974

To simulate a real earth scan situation a very high resolution satellite photograph was used (Gemini) of an area covering the Canary Islands. This image was divided into 10,000 (100 x 100) resolution elements ($\approx$ 0.1 mr) and each element was assigned one of nine alphanumeric characters which best fit the physical characteristics of that FOV (Field of View). Each character described the amount of cloud cover, and if cloud was present, its height and emissivity. Two cloud types were assumed:

1) a cloud at 800 mb with emissivity of 0.80
2) a cloud at 350 mb with emissivity of 0.85.

Each resolution element was considered to be completely cloud free or 0%, 25%, 50%, 75% or 100% cloud covered by one of the two cloud types. Thus each FOV could indicate any of nine different radiance values at a particular wavelength.

Radiance values were computed for a wave number of 875 cm^{-1} for each of the two cloud types and the completely clear situation based on upper air soundings in the vicinity of the Canary Islands at a time nearest to that of the Gemini image. These results were then used to compute the nine FOV character representations. A grid of the alphanumeric characters was punched onto computer cards along with the table of values represented by each character.

Figure 1 shows a photo facsimile of the radiances thus represented by the Gemini image. This image was generated by software which read the alphanumeric grid, interpreted each element's radiance equivalence, and assigned a grey scale value to that radiance for outputing to the facsimile machine.

A program simulator was developed to test the effectiveness of corrective

Figure 1 - Photo facsimile of Radiance image used as input in simulator

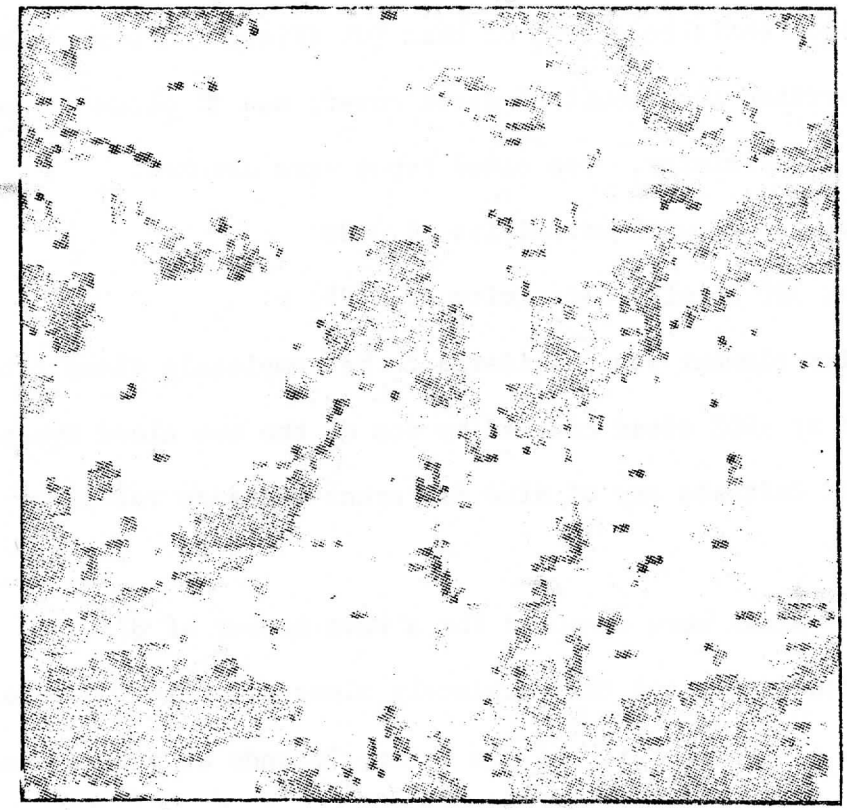

weighting of small detector fields so as to more closely match the area seen by the large detector for various configurations of north south misregistration. The program executes the following sequence of events in this order.

1) The alphanumeric grid of characters representing the Gemini image is read in while preserving spatial relationships between FOV's.

2) The table of radiance values representing the nine different characters is read in.

3) The alphanumeric grid is converted to the proper radiances by table look up for the wave number being evaluated.

4) A factor representing the fractional part of each 0.1mr FOV of misalignment is read in.

Resultant radiances are computed to represent large detector IFOV's (.4mr) by averaging small FOV's (0.1mr) utilizing the following equations where:

I_T = true radiance

I_{UNCOR} = uncorrected resultant radiances with misregistration errors

I_{COR} = corrected (by algorithm) resultant radiances

I = radiance of each small FOV (.1mr)

δ = factor read in as stated in step 4.

Figure 2 shows the form of the high resolution grid and indexing conventions.

5) True radiance

$$I_T = \left\{ (1 - \delta)\left[\sum_{k=1}^{4} I(1,k) \right] + \sum_{i=z}^{4} \sum_{k=1}^{4} I(i,k) + \delta\left[\sum_{k=1}^{4} I(5,k) \right] \right\} \frac{1}{16}$$

6) Uncorrected resultant radiance

$$I_{UNCOR} = \frac{1}{16} \sum_{i=1}^{4} \sum_{k=1}^{4} I(i,k)$$

Figure 2 Spatial Distribution of High Resolution Input Grid (0.1mr) Showing Indexing Conventions

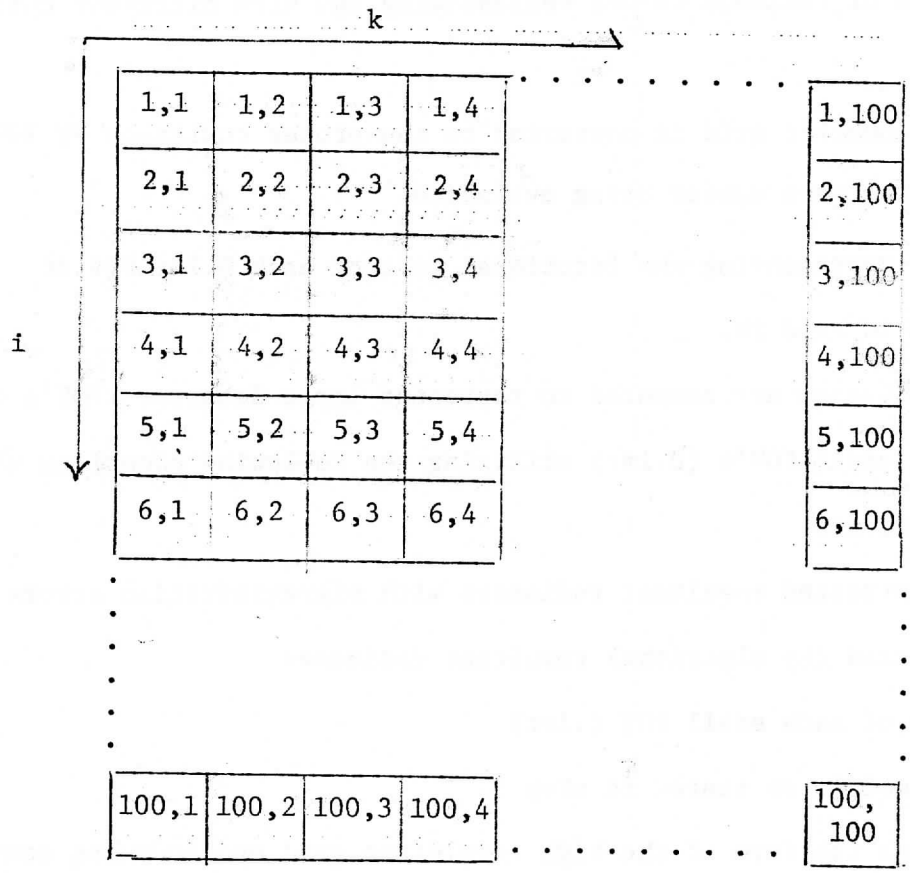

7) Corrected resultant radiance

$$I_{COR} = \left\{ \left[\sum_{i=3}^{4} \sum_{k=1}^{4} I(i,k) \right] + \left(1 - \frac{\delta}{2}\right) \left[\sum_{i=1}^{2} \sum_{k=1}^{4} I(i,k) \right] + \frac{\delta}{2} \left[\sum_{i=5}^{6} \sum_{k=1}^{4} I(i,k) \right] \right\} \frac{1}{16}$$

Steps 5, 6, and 7 are repeated to cover FOV's for the maximum image area possible.

8) Results are evaluated by comparing radiances for each large FOV evaluated by each of the two methods computed in step 6 and step 7 to that of step 5.

9) Resultant RMS errors are evaluated for the whole grid.

10) Individual errors are plotted via x-y digital plotter.

The above steps were executed for several misregistration factors. Table 1 summarizes these along with RMS errors. Figure 3 shows a graph of RMS errors of corrected and uncorrected results for each misregistration factor. Figure 4 is an example x-y digital plot for a misregistration factor of 0.10. Since the relative relationships in errors were consistent regardless of the misregistration factor (only the magnitude changed by constant factors) this is the only plot included in this writing.

FIGURE 3 RESULTANT RMS ERROR

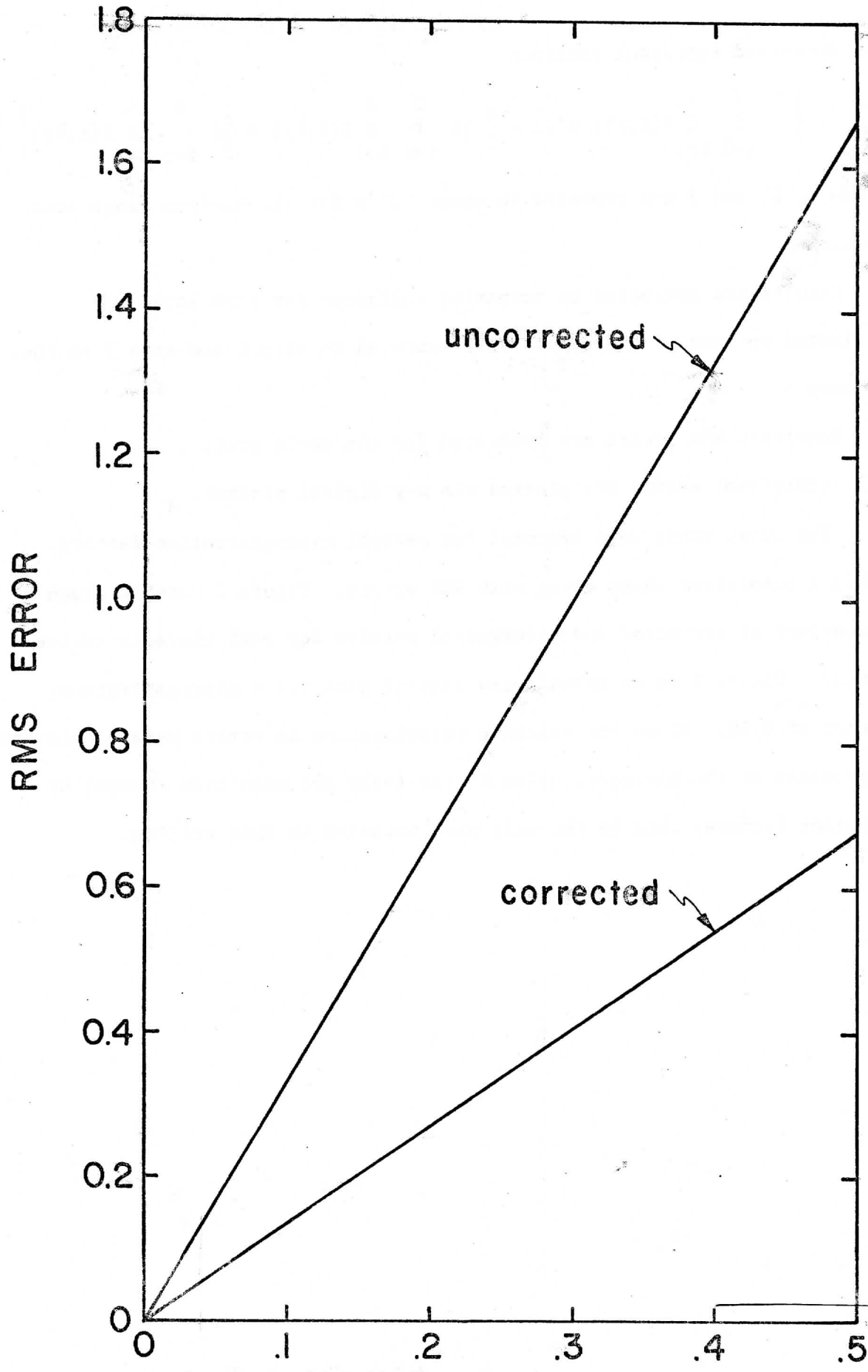

Table 1 - Summary of RMS errors over the whole grid for the various registration factors

Factor	Uncorrected RMS Error	Corrected RMS Error
0.00	0.000	0.000
0.05	0.166	0.068
0.10	0.333	0.136
0.25	0.832	0.339
0.50	1.663	0.678